University of Tehran Press

Journal of the Earth and Space Physics

Homepage: https://jesphys.ut.ac.ir

Vol. 50, No. 4, Winter 2025, P. 125-136

(Research Article)

Geometric Approach for Identifying Activated Fault Planes; Case Study: the 2014 Murmuri Earthquake, Northwestern Zagros, Iran

Abbasian, M.[1] | Rezapour, M.[2]

1. Department of Earth and Planetary Science, Rutgers, The State University of New Jersey, New Jersey, US.
2. Department of Seismology, Institute of Geophysics, University of Tehran, Tehran, Iran.

Corresponding Author E-mail: mahshad.abbasian@rutgers.edu

(Received: 20 Aug 2024, Revised: 26 Nov 2024, Accepted: 5 March 2025, Published online: 15 March 2025)

Abstract

An analysis was conducted on the 2014 Murmuri earthquake sequence in the Zagros Mountains of Iran, aiming to determine the main fault plane. The sequence comprised of an initial Mw 6.2 earthquake, followed by five aftershocks with magnitudes exceeding 5.4. Events were relocated to enhance understanding of the hypocenter uncertainties. The primary earthquake, registering a magnitude of Mw 6.2, was followed by a sequence of events with Mw>5 within 24 hours of the main shock. To identify the earthquake's source parameters, three components—local waveforms reported by the broadband networks of the Iranian Seismological Center (IRSC), the International Institute of Earthquake Engineering and Seismology (IIEES), and the Iraqi Seismological Network (ISN) were utilized. The analysis was conducted using the ISOLA software, employing a multiple-point source representation and the iterative deconvolution method. The events were relocated using the HYPOINVERSE code to ensure highly accurate results. The stations provided comprehensive coverage, contributing to the high reliability of the results. The method employed in the paper is the H-C method. This simple and readily applicable technique proves highly effective when precise information on the event location and its Centroid Moment Tensor (CMT) solution is available. The findings indicate that the Mountain Front Fault (MFF) can be identified as the causative fault plane of the event.

Keywords: Moment Tensor, Murmuri, Fault Plane, H-C Method, ISOLA.

1. Introduction

Advancements in seismic instrumentation have yielded an ever-expanding wealth of seismic data, enhancing the capability of seismologists to interpret this information more accurately. The examination and identification of source parameters and the causative fault plane in earthquake studies are crucial elements that contribute significantly to our understanding of seismotectonic processes on Earth. Focal mechanisms of earthquakes allow for the constraint of the orientation of principal stress axes, providing valuable insights into the stress state within the Earth's crust. This information is pivotal for comprehending the mechanics of earthquakes and regional deformation (Hardebeck and Hauksson, 2001). A precise interpretation of fault planes, especially in the case of intermediate-depth earthquakes–where fault planes are often unknown, as observed in the events investigated in this paper–proves essential for refining regional geodynamic models of subducted plates and stress fields (Zahradnik et al., 2008). Additionally, the identification of active crustal blind faults holds equal importance, as it can significantly enhance earthquake hazard assessment in a region (Zahradnik et al., 2008).

This study focuses on seismic events involving an Mw 6.2 main shock that occurred on August 18, 2014, triggering an earthquake sequence. This main shock was followed by five aftershocks with magnitudes exceeding 5.4 in Murmuri, located in the northwestern part of the Zagros Mountains. The Zagros Mountains (Figure 1) form a dynamically active fold-and-thrust belt, arising from the continuous collision between the Arabian Plate and the continental crust of Central Iran. This collision began during the Miocene epoch and continues to the present, with a north to north-northeast trend at velocities ranging from approximately 23–25 to 35 mm/year (Hatzfeld et al., 2003; Berberian, 1976; Jackson and McKenzie, 1984; DeMets

Cite this article: Abbasian, M., & Rezapour, M. (2025). Geometric Approach for Identifying Activated Fault Planes; Case Study: the 2014 Murmuri Earthquake, Northwestern Zagros, Iran. *Journal of the Earth and Space Physics*, 50(4), 125-136. DOI: http//doi.org/10.22059/jesphys.2025.380701.1007623

E-mail: (2) rezapour@ut.ac.ir

Publisher: University of Tehran Press.
DOI: http//doi.org/10.22059/jesphys.2025.380701.1007623

Print ISSN: 2538-371X
Online ISSN: 2538-3906

et al., 1990; Walker and Jackson, 2002; McClusky et al., 2003; Vernant et al., 2004; Rezapour and Mottaghi, 2018). Spanning approximately 2000 kilometers, the Zagros fold-thrust belt extends from southern Turkey through northern Syria and Iraq to western and southern Iran. Recognized for its abundance of supergiant hydrocarbon fields, it ranks as the most resource-rich fold-thrust belt globally, featuring several prominent thrust faults including the High Zagros fault, the Mountain Front fault (MFF), the Dezful Embayment Fault (DEF), and the Zagros Foredeep Fault (ZFF) (Figure 1) (Alavi, 2004; Berberian, 1995; Sepehr and Cosgrove, 2005; Zamani and Agh-Atabai, 2009).

Seismic activity within the Zagros belt is localized between the Main Zagros Thrust and the Persian Gulf. Larger earthquakes primarily occur on steeply inclined reverse planes oriented parallel to the trend of the fold axes. (Jackson, 1980; Jackson and McKenzie, 1984; Ni and Barazangi, 1986). Strong earthquakes are thought to occur on "blind" active thrust faults (Berberian, 1995), which are not exposed to the Earth's surface. The centroid depths of moderate-sized earthquakes across the Zagros Mountains, as determined by body wave modeling (Jackson and Fitch, 1981; Baker et al., 1993; Maggi, et al., 2000), typically range from approximately 8 to 20 km. Notably, there is no evidence of seismic activity in the mantle (Maggi, et al., 2000), suggesting a lack of direct indication of ongoing subduction in the present day. Earthquakes with moderate magnitudes ranging from M_b 5.5 to 6.0 are frequently observed within the zone spanning approximately 250 to 350 km wide along the Zagros fold-and-thrust belt (Jackson, 1980; Berberian, 1995). Although the precise localization of most earthquakes within the belt remains challenging using teleseismic data (Jackson and Fitch, 1981; Ni and Barazangi, 1986), studies suggest that seismic activity is primarily restricted to depths shallower than 40 km (Maggi et al., 2000).

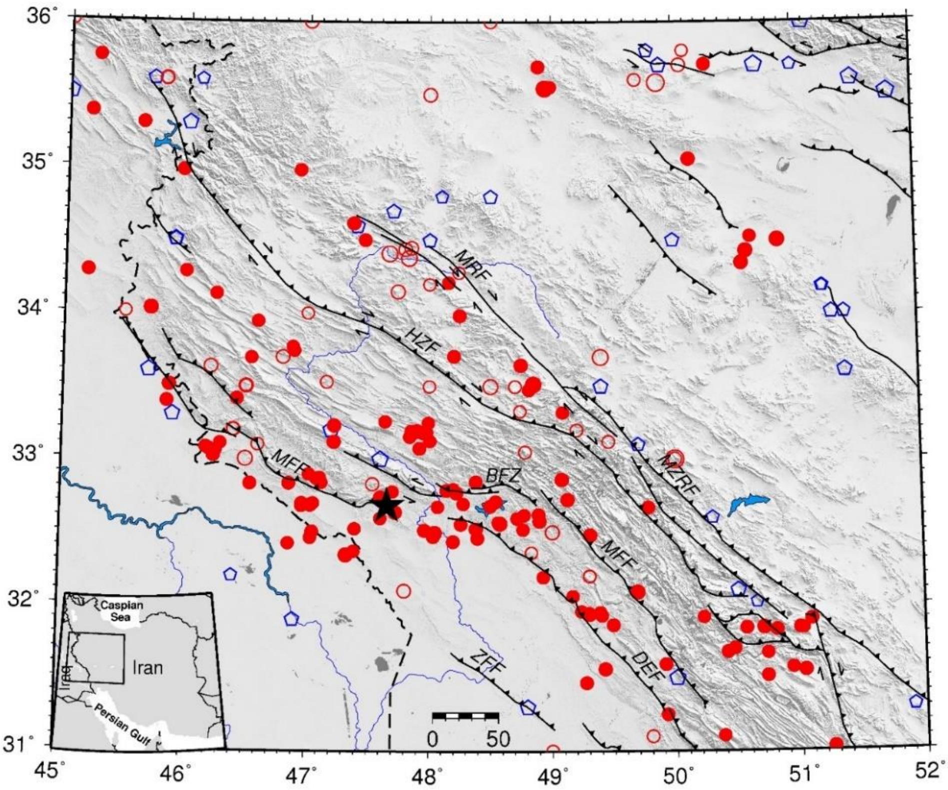

Figure 1. Seismicity map of the Zagros Mountains. The blue pentagons represent the epicenters of historical events with M ≥ 5.0. Open red circles indicate the epicenters of the first-period (1901-1963) instrumental events with magnitudes greater than or equal to 5.0. The filled red circles represent the second-period instrumental events with magnitudes greater than or equal to 5.0, which were extracted from the International Seismological Centre (ISC, 1964–2005) and Iranian Seismological Centre (IRSC, 2006–2014) bulletins. The black star indicates the epicenter of the 2014 M_W 6.2 Murmuri earthquake. All of the events are scaled according to their magnitude. The solid lines show traces of major active faults in the region. MRF, Main Recent fault; MZRF, Main Zagros reverse fault; HZF, High Zagros fault; BFZ, Balarud fault zone; MFF, Mountain Front fault; DEF, Dezful embayment fault; and ZFF, Zagros foredeep fault (Berberian, 1995; Hessami et al., 2003).

This paper explores the earthquake sequence in western Zagros during August 2014, aiming to determine the earthquake's source parameters, focal mechanisms, and, specifically, to investigate the main fault plane of the six events in the sequence. Subsequently, through the analysis of both aftershocks and the main event, we propose the slip distribution of the region. Figure 1 illustrates the seismicity map of the area, highlighting the major faults in the Zagros Mountains.

The main shock of the sequence occurred on August 18, 2014, at 02:32:04.7, preceded by foreshocks with magnitudes of M_w 4.6 and 4.5, serving as alerts for residents to evacuate the area. While we surveyed all six events, our focus is on presenting results for the two significant events: the main shock (M_w 6.2) and the largest aftershock (M_w 5.9), which occurred approximately 16 hours after the main shock. This comprehensive study of the event sequence offers seismologists valuable insights into the seismic behavior of the Zagros' fold-and-thrust belt.

2. Methodology

The determination of the main fault plane in earthquake focal mechanisms is crucial in seismotectonic studies, as it provides valuable insights into the seismic processes. Various methods exist for identifying the main fault plane, and one such approach involves finite-extent source models, particularly applicable when near-fault records are accessible. This method, although feasible with limited stations, is susceptible to location errors and introduces complexities in the rupture process (Delouis and Legrand, 1999). Alternative methods for identifying the main fault plane rely on field studies and commonly used seismological methods, such as precisely locating aftershocks. However, these approaches often require significant time and resources. In this paper, we employed the H-C geometric method, a straightforward and immediately applicable technique that relies on reliable earthquake location information and its Centroid Moment Tensor (CMT) solution (Zahradnik et al., 2008). By applying the H-C method as suggested by Zahradnik et al. (2008), our objective was to discern the main fault plane of the earthquake sequence that occurred on August 18, 2014. We examined all six events with magnitudes greater than 5.4, but we specifically present the results for the main shock (M_w 6.2) and its largest aftershock (M_w 5.9), respectively.

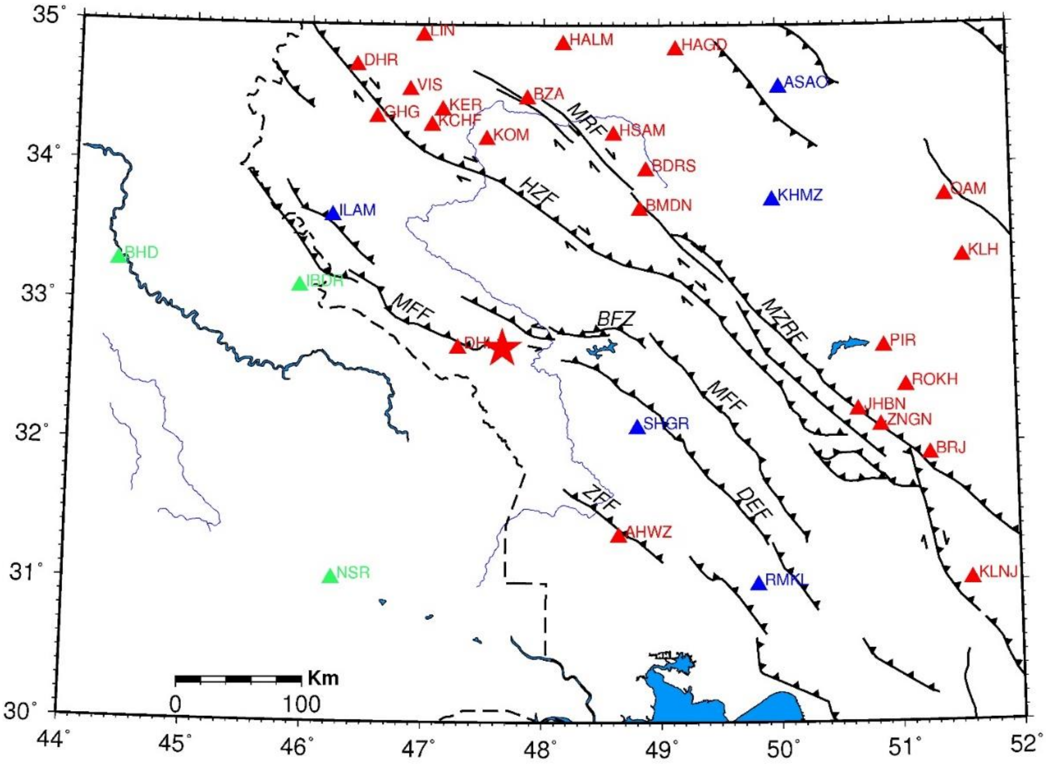

Figure 2. Seismic stations used in the relocating procedure and MT inversion. Red triangles denote the IRSC seismic network, blue triangles are associated with the IIEES, and the green ones represent the Iraqi Seismological Network. The red star marks the Murmuri main shock.

In this study, we employed the ISOLated Asperities (ISOLA) software (Sokos and Zahradnik, 2008) for waveform inversion, implementing the Centroid Moment Tensor (CMT) solution on a local scale using available data from seismic stations that belong to the IRSC, IIEES and INS (Figure 2). The methodology utilized is based on iterative deconvolution, a technique originally introduced by Kikuchi and Kanamori (1991). This study utilized data from multiple seismic stations in western Iran, but not all seismograms were included. The decision to limit the data set was based on several factors: only high-quality waveforms from reliable stations were chosen to ensure accuracy, while data from stations with technical issues or incomplete data were excluded from the waveform inversion and CMT analysis. Additionally, stations providing optimal azimuthal coverage were prioritized for the inversion procedure.

The H-C method relies on the earthquake Centroid Moment Tensor (CMT) solution, assuming a planar fault plane (Zahradnik et al., 2008). To apply this method, the initial step involves relocating the hypocenter (H) and Centroid (C) positions. The hypocenter, the point where rupture propagation initiates, is determined based on travel times. In contrast, the Centroid, representing the point source approximation where dominant slip on the fault occurs, is identified through the CMT solution using comparatively long-period waveforms (Zahradnik et al., 2008). The CMT solution provides two nodal planes passing through the Centroid, and the main fault plane is the one intersecting both the Centroid and the hypocenter. Successful application of the method requires reasonably accurate determinations of H and C positions, a sufficient distance between H and C positions (larger than individual errors of H and C positions), and earthquake geometry that is not overly complex (Zahradnik et al., 2008).

The earthquakes were relocated using the HYPOINVERSE locating program (Havskov and Ottemöller, 2005; Klein, 1984) based on P-arrival times and the IRSC velocity model. Subsequently, the centroid position and focal mechanism of the events were determined in three stages. Initially, optimal depths were identified by exploring various source depths below the hypocenter for each event. In the next stage, horizontal fault planes were defined at the optimal depth, incorporating multiple points for each event along the strike and dip in both south-north and east-west directions. Finally, in the last stage, the horizontal network was rearranged in the centroid's optimal position based on the results of the second stage to achieve a more precise outcome. The obtained results related to hypocenter and centroid positions, along with the focal mechanisms, are presented in Table 1. The analysis utilized waveforms recorded by 17 local stations, providing comprehensive coverage of the events. The method is grounded in the earthquake's Centroid Moment Tensor solution, assuming a planar fault plane.

3. Observations

3-1. M_W 6.2 Murmuri Earthquake

The geometrical H-C method, along with local and regional waveform modeling, has been employed to ascertain the causative fault plane of the M_w 6.2 earthquake that occurred on August 18, 2014, in the northwestern part of the Zagros Mountains. This seismic event, identified as the main shock in an earthquake sequence, was centered at 32.70° N and 47.67° E, based on the findings of this study. Occurring at 02:32:04.7 UTC near Murmuri, situated within the Zagros Mountains of Iran, in the Iran-Iraq Border Region, the event registered a Moment Magnitude of 6.2 and reached a maximum Mercalli intensity of VIII. The earthquake resulted in severe damages in the region, impacting approximately 17,000 houses to varying extents. Around 330 people were injured, and the shaking waves were felt even in Kuwait. The event was followed by several moderate-sized aftershocks with a magnitude greater than 5.4, occurring approximately three hours after the mainshock.

The initial step involved determining the hypocenter's location by applying the HYPOINVERSE code to invert manual P and S picks from seismic stations (Figure 2). To assess uncertainty, multiple calculations were conducted, considering four different crustal models (Hatzfeld et al., 2003; IRSC; IIEES), various starting depths, and changes in stations at different distances. The preferred hypocenter solution in this paper, utilizing the best-fitting crustal model of IRSC, developed by the Iranian Seismological Center, is presented in Table 2.

Table 1. Preferred Hypocenter Solution of this Study (Crustal model of IRSC).

Time (UTC)	Lat N (°)	Long E (°)	Depth (km)
2:32:4.7	32.702	47.665	13.0

Table 2. Iranian Seismological Center (IRSC) Crustal Model.

Depth (km)	V_P (km/s)	V_S (km/s)	Density (gr/cm3)
0	5.38	3.056	2.776
7	5.95	3.379	2.89
12	6.15	3.496	2.93
20	6.42	3.648	2.984
47	8.06	4.58	3.312

During the CMT solution phase, the comprehensive analysis involved examining broadband records from three local seismological networks: IRSC, IIEES, and INS. Subsequently, three-component waveform records from seven nearby regional stations were utilized for the MT inversion process, ensuring complete azimuthal coverage of the event (Figure 3). Notably, specific components were excluded from consideration, namely the vertical NS and horizontal ES components of the NSR station, as well as the EW and Z components of the BHD station. For the NSR and BHD stations, only the Z and NS components, respectively, were considered in the analysis.

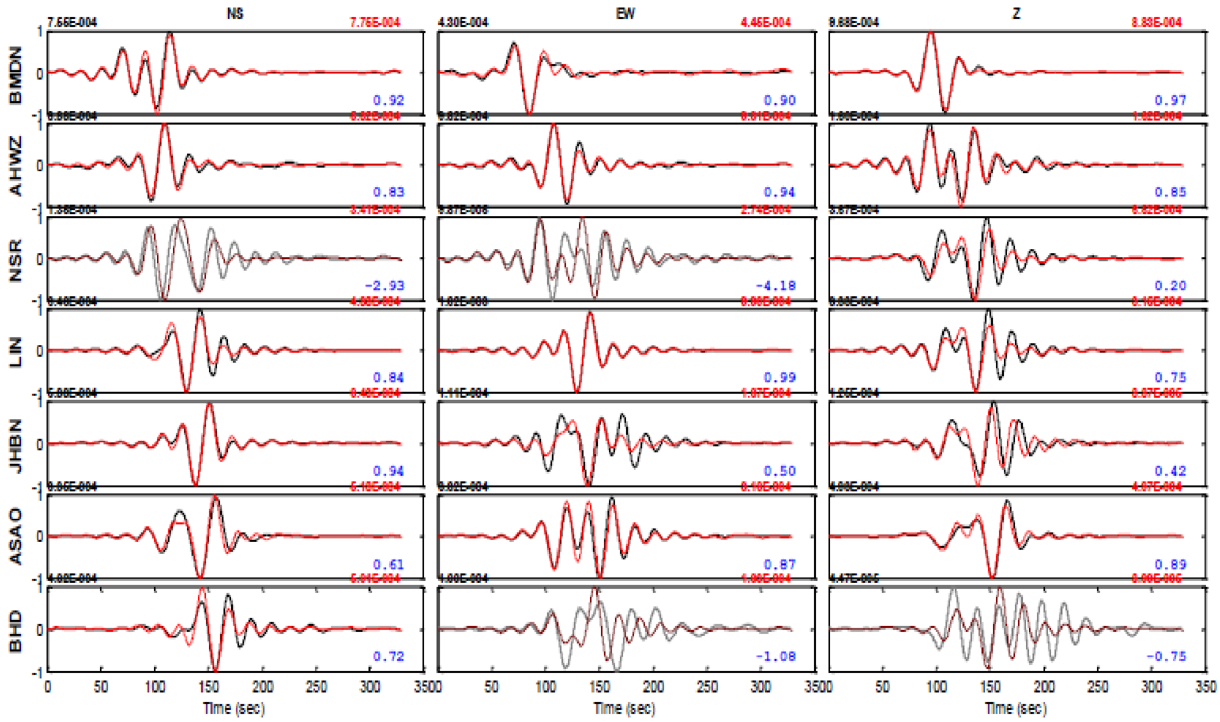

Figure 3. The waveform comparison is depicted with observed waveforms in black and synthetic waveforms in red, showcasing the preferred Centroid Moment Tensor (CMT) solution. Gray waveforms, excluded from the inversion process, are also shown.

The displacement inversion band ranged from 0.015 to 0.065. The centroid and focal mechanisms were then determined through a three-stage grid search. Initially, utilizing the ISOLA software (Sokos and Zahradnik, 2008), sources were distributed across 20 depths (with a 1 km increment) beneath the hypocenter. The preliminary inversion outcomes pointed to the most favorable results within a depth range of 3 to 9 km. Subsequently, a Centroid grid search was conducted within an 8×8 horizontal stencil (with a 7 km increment) at eight depths spanning from 3 to 9 km, encompassing a comprehensive 3-D grid search. Across all depths, the optimal position consistently emerged 7 km east of the hypocenter. The entire procedure was iteratively performed multiple times, with variations in the inclusion or exclusion of different components from the seven stations, aiming to achieve the best match. To validate the stability of the MT solution, a systematic approach was adopted, involving the removal of one station at a time, reiterating the determination of the C position and its corresponding strike, dip, and rake. The optimized solution yielded the following results (Figure 4): The centroid marks the focal point of the earthquake rupture, situated at 32.6839°N latitude and 47.657°E longitude. The seismic event transpired 6.0 seconds after the origin time. Calculated with a moment magnitude (Mw) of 6.2, the earthquake released a moment of 2.003 × 10^18 Newton-meters, with double-couple (DC%) and compensated linear vector dipole (CLVD%) components at 63.3% and 36.7%, respectively. The variance reduction, a measure of the fitting quality, is determined to be 0.88. Nodal planes define two distinct orientations: the first with a strike of 308°, dip of 36°, and rake of 102°, and the second with a strike of 113°, dip of 55°, and rake of 81°. The principal axes of the earthquake moment tensor reveal the P-axis azimuth at 210° with a plunge of 10°, and the T-axis azimuth at 354° with a plunge of 78°. Detailed moment tensor components include Mrr: 1.633, Mpp: -0.208, Mrp: -0.186, Mtt: -1.424, Mrt: 0.669, and Mtp: 1.078. The exponent of the moment tensor is specified as 18 Nm. Collectively, these parameters provide significant insights into the seismic source mechanism and the characteristics of the earthquake event.

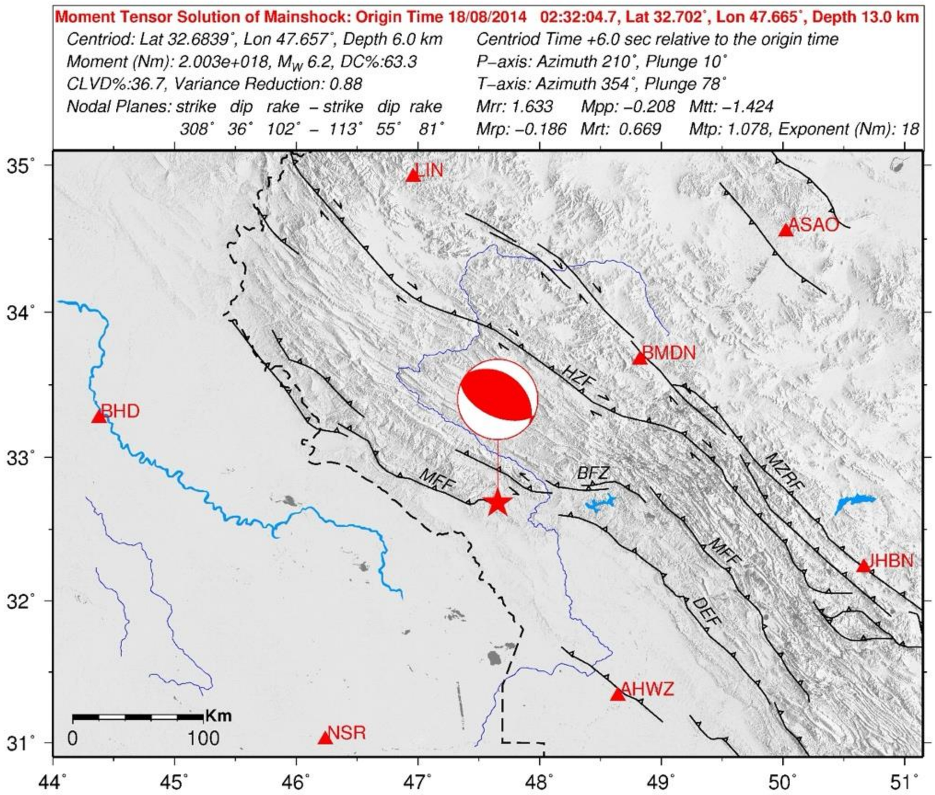

Figure 4. The outcomes for the favored MT solution in the main-shock MW 6.2. The details of the moment tensor solution, nodal planes and etc. are presented in the box above the figure. The red triangles show the seismic stations used in MT inversion.

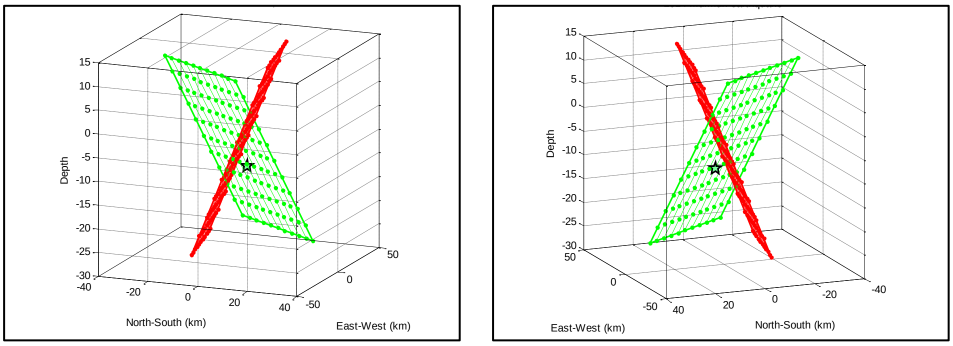

Figure 5. Tests of the H-C method. The Centroid is located at the intersection of nodal planes I and II. A plane with a strike 308°and a dip of 36° (green screen) is displayed as the main fault in the Murmuri main shock on August 18, 2014, at 2:32:04.7. The green star indicates the Hypocenter position determined in this paper.

As mentioned above, the nodal planes of the Murmuri earthquake exhibit a significant disparity in their strike and dip values. Plane I displays a dip of 36° and a strike of approximately 308°, while Plane II has a dip of 55° and a strike of 113°. Upon comparing the positions of the planes with the Hypocenter solution in Figure 6, it becomes evident that the hypocenter aligns more closely with Plane I, which has the lower dip.

3-2. M_W 5.9 Aftershock

This event, identified as the largest aftershock occurring 16 hours after the main shock, underwent all three stages similar to the main shock to determine the earthquake focal mechanism and Centroid position. Sources were distributed across 12 depths (with a 2 km increment) beneath the Hypocenter. Initial inversion results pointed to the most favorable outcomes within a depth range of 2 to 8 km. Subsequently, a Centroid grid search was conducted within an 8×8 horizontal stencil (with a 7 km increment) at seven depths ranging from 2 to 8 km, encompassing a comprehensive 3-D grid search. Across all depths, the optimal position consistently emerged 7 km west of the hypocenter. The entire procedure was iteratively performed multiple times, with variations in the inclusion or exclusion of different components from the seven stations, aiming to achieve the best match (Figure 6). To validate the stability of the MT solution, a systematic approach was adopted, involving the removal of one station at a time, reiterating the determination of the C position and its corresponding strike, dip, and rake. At the end, the favored solution, considering waveform match and H-C consistency, is presented in Figure 7, along with the illustrated results of the H-C solution.

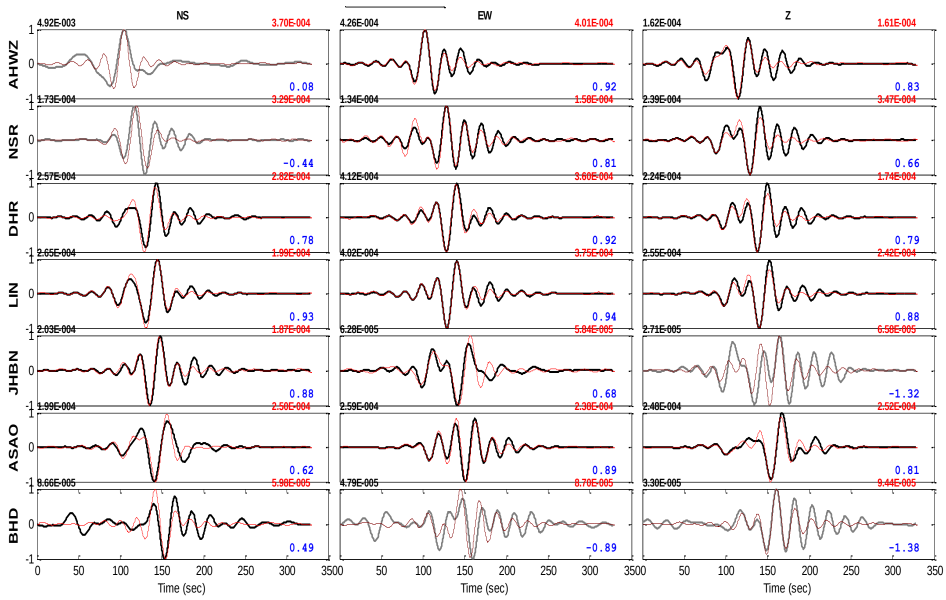

Figure 6. Comparison of waveforms between observed (black) and synthetic (red) waveforms for the preferred Centroid Moment Tensor (CMT) solution for the M_W 5.9 aftershock. Gray waveforms were excluded from the inversion process.

The centroid solution in this study for this seismic event yielded the following parameters: The centroid is located at 32.5829°N latitude and 47.6639°E longitude, with a depth of 4.0 km below the Earth's surface. The earthquake occurred 3.4 seconds after the origin time. The moment magnitude (Mw) is calculated to be 5.9, corresponding to a moment release of 8.658 × 10^17 Newton meters. The moment tensor's double-couple (DC%) component accounts for 75.1% of the seismic moment, while the compensated linear vector dipole (CLVD%) component constitutes 24.9%. The variance reduction, indicating the goodness of fit, is determined to be 0.86. Two nodal planes are identified, with the first plane having a strike of 83°, a dip of 53°, and a rake of 50°; and the second plane with a strike of 316°, a dip of 51°, and a rake of 131°. The principal axes of the earthquake moment tensor are delineated, with the P-axis having an azimuth of 200° and a plunge of 1°; and the T-axis with an azimuth of 291° and a plunge of 59°. The moment tensor components are provided, including Mrr: 6.437, Mtt: -6.850, Mpp: 0.413, Mrt: 1.695, MRP: 4.227, and Mtp: 3.153. The exponent of the moment tensor is indicated to be 17 Newton meters. These parameters collectively provide insights into the seismic source mechanism and characteristics of the earthquake event.

Applying the H-C method (Zahradnik et al., 2008) and constructing a three-dimensional focal mechanism, where H and C are positioned on the main fault plane, the plane with a strike of 316 ° and a dip of 51° is identified as the causative fault plane (Figure 8). The obtained focal mechanism in this study reveals a strike-slip with a thrust component.

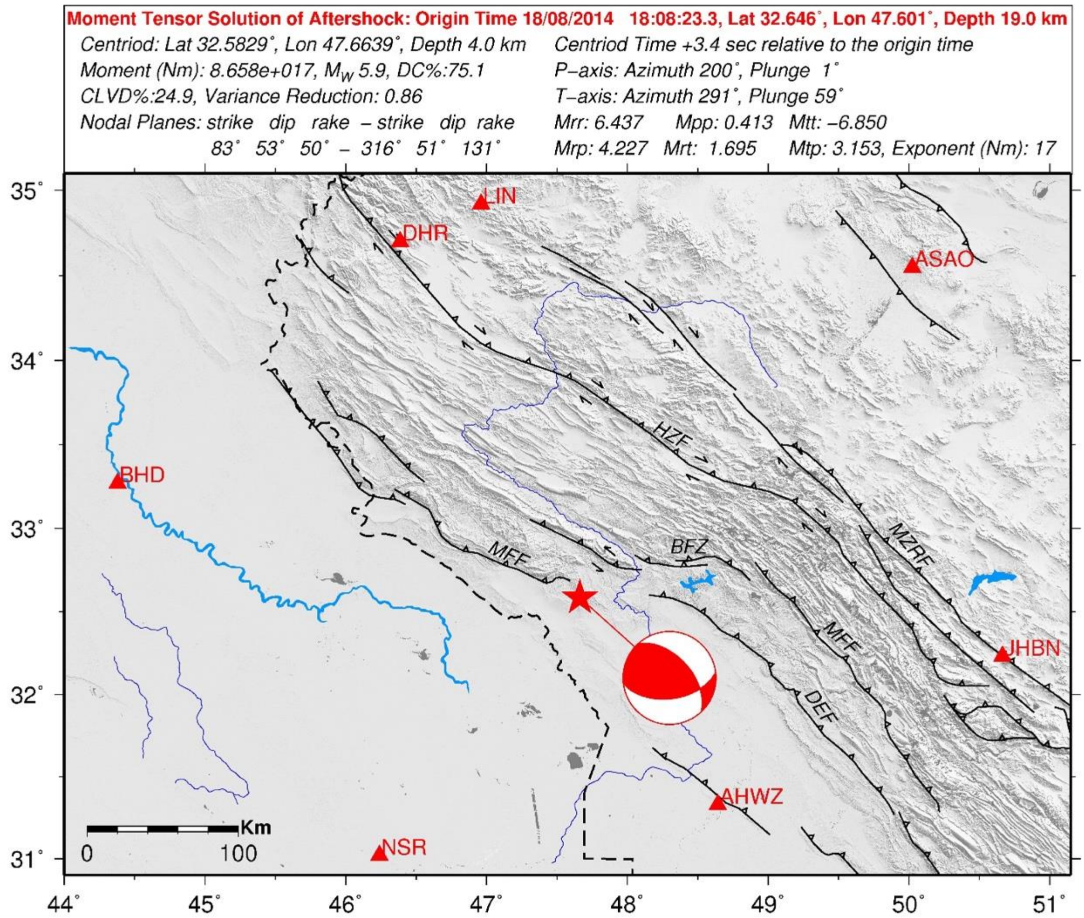

Figure 7. The outcomes for the favored MT solution in the aftershock M_W 5.9. The details of the moment tensor solution, nodal planes, and other parameters are presented in the box above the figure. The red triangles show the seismic stations used in MT inversion.

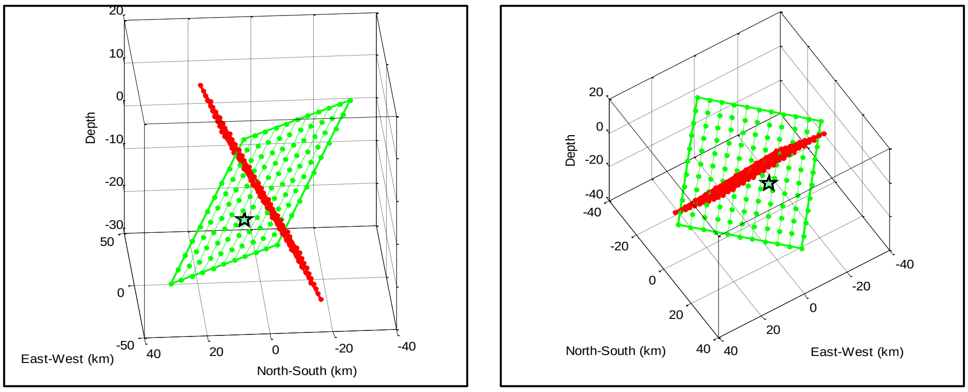

Figure 8. Evaluation of the H-C method: The Centroid is positioned at the intersection midpoint of nodal planes I and II. A plane with a strike of 316° and a dip of 51° (green screen) is displayed as the main fault in Murmuri large aftershock M_W 5.9, which occurred on August 18, 2014, at 18:08:23.3. The green star denotes the Hypocenter position obtained in this paper.

The reported centroid coordinates and focal mechanisms by seismological centers for the Murmuri M_W 6.2 earthquake and its largest aftershock M_W 5.9 are compared in Table 3. A comparison of the parameters listed in Table 3 shows that the mechanisms and centroid coordinates reported by different agencies and authors are generally consistent. The main difference is observed in the centroid depth. The USGS and GCMT have reported a larger value for centroid depth, while in this study and IRSC, a shallower depth has been determined for the centroid. This discrepancy could be attributed to differences in the crustal model, method, and data used for MT inversion. The USGS and GCMT use a global velocity model and teleseismic data, whereas this study and the IRSC have used a local crustal model and local data.

4. Discussion

The seismicity preceding the 2014 Murmuri earthquake exhibited moderate activity, dominated by minor tremors and infrequent moderate earthquakes. Historical seismic records indicate a pattern of sporadic events, primarily of low magnitudes (below Mw 5.0), with only a few larger earthquakes exceeding this threshold. This low-intensity seismicity fostered a perception of limited seismic risk among local communities, influencing both public awareness and preparedness measures. Consequently, the structural resilience of buildings and infrastructure remained insufficient for the eventuality of a major earthquake.

The Murmuri earthquake (Mw 6.2) represented a pivotal event in the seismic history of the region, significantly altering the local seismic regime. The earthquake was initiated along the Mountain Front Fault (MFF), a critical structure in the Zagros fold-and-thrust belt. The foreshocks preceding the main shock (Mw 4.6 and Mw 4.5) offered early warning signals that facilitated limited evacuation efforts, demonstrating the potential utility of real-time seismic monitoring. However, the widespread aftershock sequence, which included several events of moderate magnitudes, revealed the cascading effects of stress redistribution in the crust following the main event.

Table 3. The reported centroid coordinate and focal mechanism by different seismological agencies, for the Murmuri M_W 6.2 earthquake and its largest aftershock M_W 5.9.

	Agencies*	Origin Time hh:mm:ss.s	Centroid Lat. (°)	Centroid Lon. (°)	Centroid Depth (km)	Moment Magnitude	Strike/Dip/Rake (°)
Mainshock 2014/08/18	IRSC	02:32:04.1	32.65	47.69	5.0	M_W 6.2	320/32/121 & 104/53/72
	USGS	02:32:05.0	32.703	47.695	11.5	M_W 6.2	310/19/100 & 119/72/87
	GCMT	02:32:04.3	32.59	47.53	12.0	M_W 6.2	317/27/111 & 114/65/80
	This study	02: 32:04.7	32.6839	47.657	6.0	M_W 6.2	308/36/102 & 113/55/81
Aftershock 2014/08/18	IRSC	18:08:24.0	32.6291	47.6643	4.0	M_W 5.9	305/52/109 & 97/42/68
	USGS	18:08:22.0	32.583	47.704	11.5	M_W 6.0	312/29/140 & 78/72/67
	GCMT	18:08:22.7	32.50	47.57	12.0	M_W 6.0	300/30/108 & 99/62/80
	This study	18:08: 23.3	32.646	47.601	4.0	M_W 5.9	311/51/131 & 83/53/50

*Agencies: IRSC, Iranian Seismological Center; USGS, U.S. Geological Survey; GCMT, Global Centroid Moment Tensor.

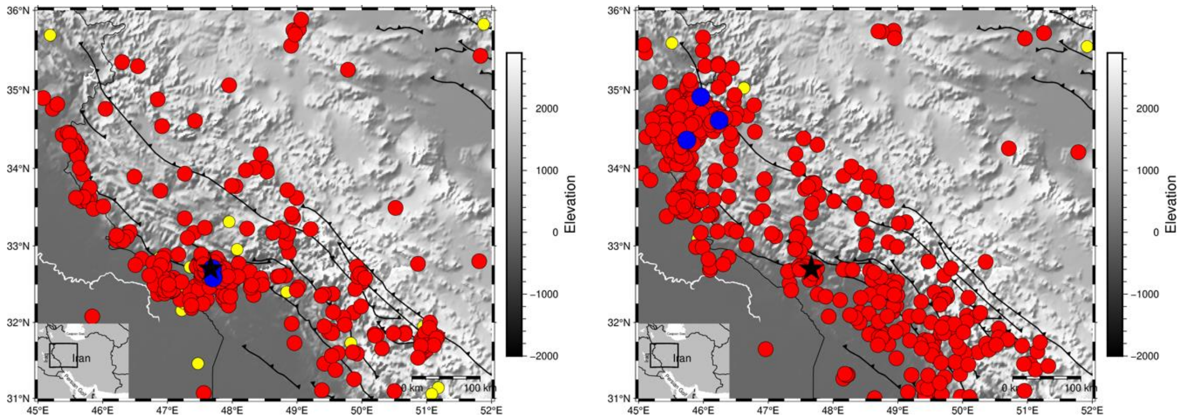

(a) (b)

Figure 9. Depicts the seismicity patterns prior to (a) and following (b) the Murmuri main event. The map represents seismic activity spanning eight years before (a) and eight years after (b) the main event. Events are color-coded based on magnitude: blue for events exceeding magnitude 6, red for moderate events with magnitudes between 4 and 6, and yellow for smaller events below magnitude 4.

Our analysis of the post-2014 seismicity indicates a substantial increase in earthquake frequency and intensity in the western part of Zagros Mountain (Figure 9). This shift can be attributed to the reactivation of nearby faults triggered by redistributing tectonic stresses. The activation of these faults underscores the dynamic response of the region's fault systems to significant seismic events. Moreover, the high-resolution seismic data from IRSC, IIEES, and ISN networks allowed for precise determination of the earthquake source parameters, reinforcing the importance of well-distributed seismic monitoring networks for studying complex tectonic settings.

The results of this study provide critical insights into the seismotectonic behavior of the Zagros Mountains. The seismic activity in this region is confined to the crust, consistent with the absence of active subduction. This observation aligns with previous studies and highlights the role of blind thrust faults as primary contributors to the region's seismic hazards. Identifying the MFF as the causative fault advances our understanding of fault mechanics and the stress regime within the Zagros fold-and-thrust belt.

The findings emphasize the need for updated seismic hazard assessments and mitigation strategies. The heightened seismic activity following the Murmuri earthquake signifies an elevated risk for future events, particularly along nearby fault systems. Regional building codes should incorporate these findings to enhance structural resilience, and public education programs must focus on improving awareness of earthquake risks and preparedness.

Despite the advancements in seismic instrumentation and analysis, challenges remain in accurately localizing seismic events within the complex geological structures of the Zagros region. Future studies should focus on integrating more extensive seismic networks and employing advanced modeling techniques to reduce fault behavior and stress interaction uncertainties.

5. Conclusion

Utilizing both local and regional data proved instrumental in achieving greater precision during waveform modeling. Accurate identification of the hypocenter and centroid positions facilitated the determination of the main fault plane. From a geological perspective, Ilam province is situated within the Zagros fold-and-thrust belt or its external basin. The region stands out in seismotectonic terms due to significant faults. Before the Murmuri earthquake, the area was generally perceived to have either low or medium seismic hazard potential. Considering recent events, it is evident that a comprehensive assessment of seismic hazards and risks in the region is now imperative.

Comparing our study with previous research conducted by Motagh et al. (2015) and Copley et al. (2015) highlights contrasting views on the seismicity of the Ilam province. While our investigation primarily focuses on accurately determining the earthquake's hypocenter and centroid positions using waveform modeling, Motagh et al. (2015) emphasized the uplift of the Dalpari anticline and faulting within the sedimentary cover. Furthermore, Copley et al. (2015) identified distinct fault planes for both the mainshock and its largest aftershock, suggesting separate rupture mechanisms. Although our findings offer complementary insights into seismic hazards and fault behavior in the region, they do not necessarily corroborate each other. Instead, they provide valuable perspectives that contribute to a more comprehensive understanding of the seismic activity in the Ilam province.

Acknowledgments

We acknowledge waveform data support from the Iranian Seismological Center (IRSC), the International Institute of Earthquake Engineering and Seismology (IIEES), and the Iraqi Seismological Network (ISN).

References

Alavi, M. (2004). Regional stratigraphy of the Zagros fold-thrust belt of Iran and its proforeland evolution. *American journal of Science*, 304(1), 1-20.

Baker, C., Jackson, J., & Priestley, K. (1993). Earthquakes on the Kazerun Line in the Zagros Mountains of Iran: strike-slip faulting within a fold-and-thrust belt. *Geophysical Journal International*, 115(1), 41-61.

Berberian, M. (1976). Contribution to the seismotectonics of Iran (part II-III): In commemoration of the 50th anniversary of the Pahlavi dynasty (No. 40). Ministry of Industry and Mines, Geological Survey of Iran, Tectonic and Seismotectonic Section.

Berberian, M. (1995). Master “blind” thrust faults hidden under the Zagros folds: active basement tectonics and surface morphotectonics. *Tectonophysics*, 241(3-4), 193-224.

Copley, A., Karasozen, E., Oveisi, B., Elliott, J.R., Samsonov, S., & Nissen, E. (2015). Seismogenic faulting of the sedimentary sequence and laterally variable material properties in the Zagros Mountains (Iran) revealed by the August 2014 Murmuri (E. Dehloran) earthquake sequence. *Geophysical journal international*, 203(2), 1436-1459.

DeMets, C., Gordon, R.G., Argus, D.F., & Stein, S. (1990). Current plate motions. *Geophysical journal international*, 101(2), 425-478.

Delouis, B., & Legrand, D. (1999). Focal mechanism determination and identification of the fault plane of earthquakes using only one or two near-source seismic recordings. *Bulletin of the Seismological Society of America*, 89(6), 1558-1574.

Hardebeck, J.L., & Hauksson, E. (2001). Stress orientations obtained from earthquake focal mechanisms: What are appropriate uncertainty estimates?. *Bulletin of the Seismological Society of America*, 91(2), 250-262.

Hatzfeld, D., Tatar, M., Priestley, K., & Ghafory-Ashtiany, M. (2003). Seismological constraints on the crustal structure beneath the Zagros Mountain belt (Iran). *Geophysical Journal International*, 155(2), 403-410.

Havskov, J., & Ottemöller, L. (2005). SEISAN Version 8.1-introductory training course. *Norway: Bergen University*.

Hessami, K., Pantosti, D., Tabassi, H., Shabanian, E., Abbassi, M.R., Feghhi, K., & Solaymani, S. (2003). Paleoearthquakes and slip rates of the North Tabriz Fault, NW Iran: preliminary results. *Annals of Geophysics*, *46*(5), 903-915.

Jackson, J. (1980). Errors in focal depth determination and the depth of seismicity in Iran and Turkey. *Geophysical Journal International*, 61(2), 285-301.

Jackson, J., & Fitch, T. (1981). Basement faulting and the focal depths of the larger earthquakes in the Zagros mountains (Iran). *Geophysical Journal International*, 64(3), 561-586.

Jackson, J., & McKenzie, D. (1984). Rotational mechanisms of active deformation in Greece and Iran. *Geological Society, London, Special Publications*, 17(1), 743-754.

Kikuchi, M., & Kanamori, H. (1991). Inversion of complex body waves—III. *Bulletin of the Seismological Society of America*, 81(6), pp.2335-2350.

Klein, F.W. (1984). User's guide to hypocenters, a program for Vax and Pc 350 computers to solve for earthquake locations. US Geol. Surv. Open-File Rept, pp.84-000.

Maggi, A., Jackson, J.A., Priestley, K., &

Baker, C. (2000). A re-assessment of focal depth distributions in southern Iran, the Tien Shan and northern India: Do earthquakes really occur in the continental mantle?. *Geophysical Journal International*, 143(3), 629-661.

McClusky, S., Reilinger, R., Mahmoud, S., Ben Sari, D., & Tealeb, A. (2003). GPS constraints on Africa (Nubia) and Arabia plate motions. *Geophysical Journal International*, 155(1), 126-138.

Motagh, M., Bahroudi, A., Haghighi, M.H., Samsonov, S., Fielding, E., & Wetzel, H.U., 2015. The 18 August 2014 M w 6.2 Mormori, Iran, earthquake: A thin-skinned faulting in the Zagros Mountain inferred from InSAR measurements. *Seismological Research Letters*, 86(3), 775-782.

Ni, J., & Barazangi, M. (1986). Seismotectonics of the Zagros continental collision zone and a comparison with the Himalayas. *Journal of Geophysical Research: Solid Earth*, 91(B8), 8205-8218.

Rezapour, M., & Mottaghi, A.A. (2018). The 18 August 2014 Mw 6.2 Murmuri, Southwest Iran, Earthquake: Aftershock Sequence Analysis. *Bulletin of the Seismological Society of America*, 108(4), 1905-1917.

Sepehr, M., & Cosgrove, J.W. (2005). Role of the Kazerun Fault Zone in the formation and deformation of the Zagros Fold-Thrust Belt, Iran. *Tectonics*, 24(5), 1-15.

Sokos, E.N., & Zahradnik, J. (2008). ISOLA a Fortran code and a Matlab GUI to perform multiple-point source inversion of seismic data. *Computers & Geosciences*, 34(8), 967-977.

Vernant, P., Nilforoushan, F., Hatzfeld, D., Abbassi, M.R., Vigny, C., Masson, F., Nankali, H., Martinod, J., Ashtiani, A., Bayer, R., & Tavakoli, F. (2004). Present-day crustal deformation and plate kinematics in the Middle East constrained by GPS measurements in Iran and northern Oman. *Geophysical Journal International*, 157(1), 381-398.

Walker, R., & Jackson, J. (2002). Offset and evolution of the Gowk fault, SE Iran: a major intra-continental strike-slip system. *Journal of structural Geology*, 24(11), 1677-1698.

Zahradnik, J., Gallovic, F., Sokos, E., Serpetsidaki, A., & Tselentis, A. (2008). Quick fault-plane identification by a geometrical method: Application to the Mw 6.2 Leonidio earthquake, 6 January 2008, Greece. *Seismological Research Letters*, 79(5), 653-662.

Zamani, A., & Agh-Atabai, M. (2009). Temporal characteristics of seismicity in the Alborz and Zagros regions of Iran, using a multifractal approach. *Journal of Geodynamics*, 47(5), 271-279.